Electron Bernstein Wave (EBW) current drive profiles and efficiency for STEP

Thomas Wilson[1], *Simon* Freethy[1], *Mark* Henderson[1], *Alf* Köhn-Seeman[2], *Ivan* Konoplev[1], *Samuli* Saarelma[1], *David* Speirs[3], *Roddy* Vann[4], and the STEP team[1]

[1] UKAEA, Culham Science Centre, Abingdon, OX14 3DB, United Kindgom
[2] University of Stuttgart, IGVP, Pfaffenwaldring 31, 70569 Stuttgart, Germany
[3] University of Strathclyde, 16 Richmond St, Glasgow, G1 1XQ, United Kingdom
[4] University of York, York, YO10 5DD, United Kingdom

Abstract. GENRAY and CQL3D were used to estimate the Electron Bernstein Wave (EBW) current drive profiles and normalised current drive efficiency ζ_{CD} (6) for several STEP reactor concepts with varying temperature, density, geometry and magnetic field. $\zeta_{CD} > 1.0$ was readily found for $\rho = 0.65 - 0.9$ while $\zeta_{CD} > 0.5$ was found for $\rho \geq 0.5$. Okhawa is found to be the most efficient current drive mechanism due to the high trapped fraction in STEP. Optimal current drive was found for 2nd harmonic absorption for $\rho \leq 0.8$ due to the higher $v_{\perp}$at the wave-particle resonance. 1st harmonic absorption is required for $\rho > 0.8$ as there is no access to the 2nd harmonic at the launch frequencies examined. Rays with negative starting $N_{\parallel}$ were found to penetrate furthest. Due to the high electron temperature in STEP the relativistic downshift of the harmonic becomes comparable to the Doppler shift, increasing access to the 2nd harmonic.

1 Introduction

The UK's Spherical Tokamak for Energy Production (STEP) reactor design program is now exclusively investigating concepts using microwave based heating and current drive (HCD) systems. Electron Bernstein Wave (EBW) HCD is a relatively immature technology compared to Electron Cyclotron (EC) HCD but is of interest due to the promise of high current drive efficiency and access to dense plasmas at low magnetic fields or high density where EC is cut off.

The general ray tracing code GENRAY [1] and bounce-averaged Fokker-Planck code CQL3D [2**Error! Reference source not found.**] were used to estimate the EBW current drive profiles and the current drive efficiency for several STEP Prototype Reactor (SPR) concepts. We aimed to find estimates of the optimal EBW current drive efficiency and gain understanding of how EBW compares to EC and what parameters limit EBW access. This is used to dimension the total required microwave power and guide design of plasma scenarios with high current drive efficiency.

The need for quick estimates and large parameter ranges on launch location and frequency necessitated a simplified modelling approach where effects such as coupling and finite beam width were ignored. This work should be therefore considered a first step used to generate an initial design for the STEP EBW scenario, which will then be further analysed using more realistic EBW models.

We find the predicted EBW current drive efficiency is nearly triple that for EC in all SPRs studied, with normalised efficiency $\zeta_{CD} > 1.0$ found for $\rho = 0.65 - 0.9$. Okhawa was the most efficient current drive mechanism for all SPRs. Optimal current drive is found for 2nd harmonic absorption where it is accessible.

The high electron temperatures in the STEP concepts produce a large Doppler broadening of the cyclotron resonance, limiting EBW access to $\rho \geq 0.5$. The relativistic downshift is also seen to be comparable with the Doppler shift. Combined with the large well in the magnetic field this allows 2nd harmonic access for an increased range of frequencies.

2 Physics Background

STEP requires a completely non-inductive current drive system which will be provided by purely microwave based HCD systems. These systems must operate as efficiently as possible to maximise net electrical power and commercial viability. We are interested in waves in between the 1st and 2nd harmonic of the electron cyclotron frequency ω_{ce}. EBWs are electrostatic electron waves, sustained by electron cyclotron motion, propagating across the magnetic field in a hot plasma. It is convenient here to define the Stix parameters X and Y for a wave at frequency ω

$$X = \left(\frac{\omega_{pe}}{\omega}\right)^2 \quad Y = \frac{\omega_{ce}}{\omega} \tag{1}$$

Compared to O and X mode, EBWs have two properties which make them appealing for a HCD system

1) The wave-particle interaction is stronger due to the electrostatic nature of the EBW compared to the electromagnetic O/X mode. This increases

the efficiency of current drive processes as energy is transferred to higher energy electrons.
2) EBWs have no density cut off and can propagate into the 'overdense' region $X > 1$.

High theoretical current drive efficiency is the primary reason for research into EBW HCD systems. STEP is currently being designed with an option for EBW heating though there is currently little experimental data for EBW current drive on tokamaks.

3 EBW Excitation

EBWs can be excited from microwaves via mode conversion of slow X mode at the Upper Hybrid (UH) layer. This can be achieved in three ways

1) Launching slow X mode from the high field side (HFS) (XB conversion).
2) Launching fast X mode from the low field side (LFS) and tunnelling onto the slow X mode (direct XB tunnelling).
3) Launching O mode from the LFS at a critical angle and converting to slow X mode at the $X = 1$ layer (OXB conversion).

In this paper we only consider LFS launch and OXB conversion as option 1 suffers from absorption of the X-mode at the fundamental harmonic and option 2 requires high density gradients that STEP will not achieve.

3.1 EBW Absorption

EBWs are absorbed very strongly compared to O and X mode due to their electrostatic nature [3]. The finite temperature of the plasma and large $N_\parallel$ leads to a large Doppler shift away from the cyclotron harmonics, where the EBW is completely absorbed on high energy electrons at the tail of the distribution far from the cold resonance.

The relativistic Doppler shifted resonance condition is [4]

$$1 = \frac{nY}{\gamma} + N_\parallel \beta_\parallel \qquad (2)$$

where γ is the Lorentz factor, $N_\parallel$ is the component of the wavevector parallel to the magnetic field $\boldsymbol{B}$ and $\beta_\parallel = \frac{v_\parallel}{c}$ is the velocity of the resonant electrons parallel to $\boldsymbol{B}$ normalised to the speed of light.

For $N_\parallel^2 < 1$ (2) traces an ellipse in $(\beta_\parallel,\ \beta_\perp)$ velocity space [4]. It is useful to compare β to the normalised thermal velocity β_T including relativistic corrections [5]. As a simple estimate we assume the EBW is only absorbed for $|\beta_\parallel| < \alpha\beta_T$, where $\alpha = 3 - 3.5$ [6]. As the EBW absorption is so strong this effectively means absorption occurs at $\beta_\parallel = \alpha\beta_T$ [7,8]. Substituting into (2) we get an estimate for the resonance condition

$$\mathrm{nY} = \frac{1 \pm \alpha N_\parallel \beta_T}{\sqrt{1 - \alpha^2\beta_T^2 - \beta_\perp^2}} \qquad (3)$$

However, the absorption of the wave is a finite Larmor radius effect. The absorption on the n-th harmonic is proportional to $\frac{J_n(\mu)}{\mu}$ [4] where J_n is the n-th Bessel function of the first kind and $\mu = k_\perp r_L$.

For the 1st harmonic this has maximum at $\beta_\perp = 0$ while for the 2nd harmonic this is zero at $\beta_\perp = 0$. Therefore, for the 1st harmonic in we set $\beta_\perp = 0$ and for the 2nd harmonic $\beta_\perp = \beta_T$. However, the value of $\beta_\perp$ has little effect on (2) as it is small compared to $3 - 3.5\beta_T$.

It should be noted for STEP the high temperature means $\beta_T \geq 0.1$ for $\rho > 0.8$ and $\beta_T \geq 0.15$ for $\rho > 0.55$, resulting in a relativistic downshift comparable with the Doppler shift.

3.2 EBW Current Drive

When the EBW is absorbed, the wave-particle interaction results in a transfer of energy to electrons, creating a perturbation in the distribution function away from pure Maxwellian, called quasilinear diffusion.

Resonant electrons can gain both perpendicular and parallel momentum from the wave. From considering conservation of energy and momentum we get [4]

$$\frac{dp_\perp}{dp_\parallel} = \left(\frac{1}{N_\parallel \beta_\parallel} - 1\right)\frac{\beta_\parallel}{\beta_\perp} \qquad (4)$$

In our cases $|N_\parallel \beta_\parallel| \sim 0.1$, meaning momentum transfer is almost completely perpendicular. This means two dominant mechanisms for current drive are the Fisch-Boozer effect [4] and the Okhawa effect [4], neither of which require parallel momentum transfer.

3.3 Current Drive Efficiency

GENRAY and CQL3D output the total toroidal driven current I_{CD} by an EBW of input power P, which allows calculation of the absolute current drive efficiency η

$$\eta = \frac{I_{CD}[A]}{P[W]} \qquad (5)$$

Current drive efficiency is typically analysed using a normalised parameter ζ_{CD} defined as [9]

$$\zeta_{CD} = 32.7\frac{\eta[A/W] n_e[10^{20} m^{-3}] R[m]}{T_e[keV]} \qquad (6)$$

where n_e is the plasma density, R is the radius of the magnetic axis and T_e is the electron temperature. This parameter allows comparison of different plasma scenarios by removing the effect of collisionality and geometry from the absolute current drive efficiency.

4 Modelling Codes and Input Data

4.1 GENRAY

GENRAY is a general ray tracing code for the calculation of electromagnetic wave propagation and absorption in the geometrical optics approximation. This code calculates the trajectory of the wave and evolution of wave parameters such as $N_{\parallel}$ and power.

All GENRAY calculations had two stages. The first is to scan over the poloidal and toroidal launch angles to find the most efficient OX conversion. There are always two solutions for positive and negative $N_{\parallel}$. The second is ray tracing at the optimal OX conversion angles. Wave power was fixed at 1MW. To speed up calculations only electron dynamics were included and we used a single ray representation (implying 100% efficient OX conversion). Our ray tracing procedure follows a similar method to [10]. The Hamiltonian used (id=6) is described here [1].

4.2 CQL3D

CQL3D is a multi-species, 2D-in-momentum-space, 1D in radial coordinate, fully relativistic, bounce-averaged, collisional-quasilinear Fokker-Planck equation solver. It calculates the resulting heating and current drive from the GENRAY ray tracing calculations.

CQL3D uses output from GENRAY to calculate the quasilinear diffusion coefficient along the ray trajectory, then calculates the flux surface averaged and bounce averaged electron distribution function resulting from the balance of wave heating, electric field effects and collisional relaxation. This allows calculation of the current driven on each flux surface.

In our cases, the Fokker Planck equation was solved on a grid of 26 flux surfaces. CQL3D outputs the total driven toroidal current and current density, which was used to calculate the current drive efficiency and the localisation of the current drive. It also outputs the electron distribution function on the midplane, which can be scaled to the magnetic field at the resonance location by transforming the pitch angle, preserving energy and magnetic moment [2], and discarding particles which fail to reach the resonance.

4.3 STEP Prototype Reactors (SPRs)

Important geometrical and plasma parameters for the considered 4 SPRs are given in Table 1. SPR-039 and SPR-045 are the same size but have different kinetic profiles. The density and temperature profiles were generated from Europed runs [10]. Z effective was set as a flat profile at 1.8.

All SPRs considered have a well in the total magnetic field on the low field side (LFS, with the minimum magnetic field occurring on midplane at $\rho \sim 0.6$, as can be seen for SPR-046 in Figure 1. This is important for the interpretation of the current drive results as launching towards the core causes Y to drop.

SPR	R_{maj} [m]	R_{min} [m]	B_{geo} [T]	$\langle n_e \rangle$ [10^{19}m^{-3}]	$\langle T_e \rangle$ [keV]
008	3.64	2.18	2	13.2	8.7
011	2.5	1.5	2.4	18.9	8.3
039	3.4	2	3.2	12.3	10
046	3.4	2	3.2	14.7	10

Table 1. Important geometrical and plasma parameters for SPRs considered in the scans.

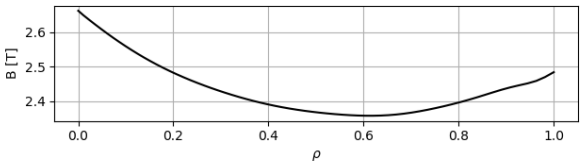

Figure 1. Magnetic field strength on midplane low field side for SPR-046. Note the minimum at $\rho \sim 0.6$ and that the field is below the value at $\rho = 1$ for $0.2 < \rho < 1.0$.

4.4 Scan Parameters

For a launch frequency f and launch height Z_L we ran GENRAY and CQL3D to find the total driven current for 1MW input power. The launcher radius was set 1m outboard from the last closed flux surface at Z_L. For each launcher height we analysed both OX solutions for positive and negative optimal $N_{\parallel}$.

For each SPR, f and Z_L were scanned over the ranges given in Table 2. The height was scanned in steps of 0.25m for Z_L and 1 GHz for f. The launcher height was only scanned above the midplane and we took the absolute value of the current when calculating efficiencies. We assume we can recover current drive of the same magnitude but with the opposite sign by launching from the opposite side of the midplane with opposite launch angles.

SPR	Z_L [m]	f [GHz]
008	0 – 3.0	66 - 88
011	0 – 2.0	66 - 88
039	0 – 3.5	73 - 97
046	0 – 4.0	73 - 97

Table 2. Scan range for launch height Z_L [m] and frequency f [GHz] for the EBW scans for each SPR.

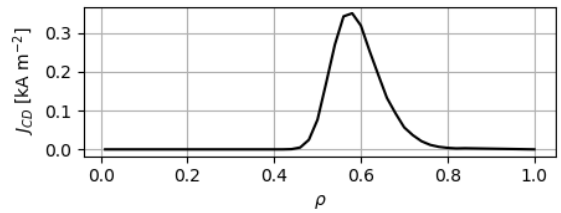

Figure 2. Driven current density profile giving maximum current drive at $\rho = 0.55$ for SPR-046. Current is driven for approximately $\rho = 0.1$ each side of the peak.

We associated the current drive efficiency with the rho value of the peak in the driven current density. The current drive profiles are not completely localised at a given ρ value though typically the bulk of the current was within $\rho = 0.1$ of the peak value, as seen in Figure 2. If the peak driven current density was less than 1 kA $m^{-2}MW^{-1}$ the efficiency was set to 0.

5 Current Drive Results

5.1 Maximum Current Drive Efficiency

The maximum ζ_{CD} for each SPR considered is shown in Figure 3. $\zeta_{CD} > 0.5$ was readily achieved for all scenarios for $\rho > 0.5$ and $\zeta_{CD} > 1$ is found for $0.6 < \rho < 0.9$. This is almost 3 times larger than the values found for EC [*L. Figini, this workshop*]. The EBW fails to penetrate the plasma beyond $\rho = 0.4$, though current drive becomes inefficient for $\rho < 0.5$.

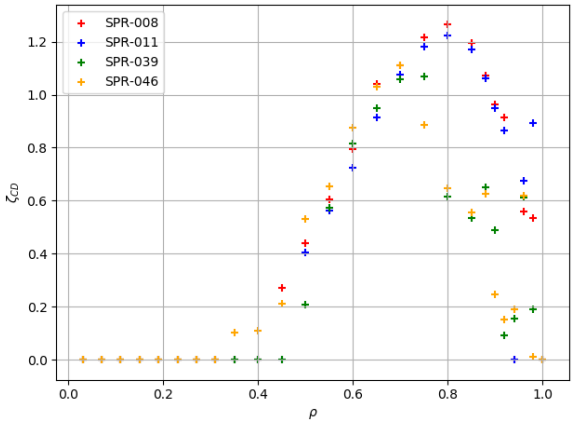

Figure 3. Maximum ζ_{CD} vs ρ of the peak in the driven current density for each SPR.

There is good agreement between all SPRs apart from between $0.7 < \rho < 0.9$ for SPR-039 and SPR-046. There were some numerical issues with these SPRs causing GENRAY to exit as the OX conversion failed. This can likely be resolved via adjustment of numerical parameters and so SPR-039 and SPR-046 are expected to agree with SPR-008 and SPR-011 in this region.

5.2 Analysis of results

To understand these results we need to study the wave particle resonance. Figure 4 shows the power damped on the 1st and 2nd harmonic from CQL3D for all SPRs.

We see a transition 1st harmonic to 2nd harmonic absorption when moving towards the plasma core. We also see the optimal current drive occurs for the positive $N_\parallel$ solution of the OX conversion for $\rho > 0.6$ and for negative $N_\parallel$ for $0.4 \leq \rho \leq 0.6$.

From (2) we see resonance $N_\parallel \beta_\parallel > 0$ for a 1st harmonic and $N_\parallel \beta_\parallel < 0$ for a 2nd harmonic resonance. From the sign of $N_\parallel$ we get the sign of $\beta_\parallel$, which can be compared to the sign of I_{CD} to figure out if the current drive is Fisch-Boozer or Okhawa. The total current drive multiplied by the sign of the resonant electron velocity is plotted in Figure 5.

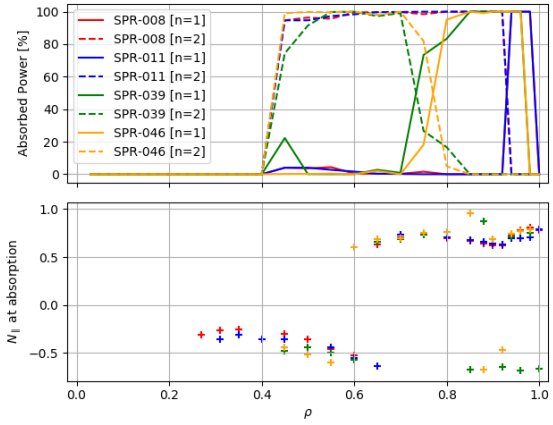

Figure 4. Percentage of total power absorbed on the 1st and 2nd harmonic (top) and $N_\parallel$ at absorption for each SPR. There is a transition from 1st harmonic absorption to 2nd harmonic. This transition is further inboard SPR-039 and SPR-045. Rays with best access have negative $N_\parallel$. Note the SPR-008 and SPR-011 traces overlay each other (top).

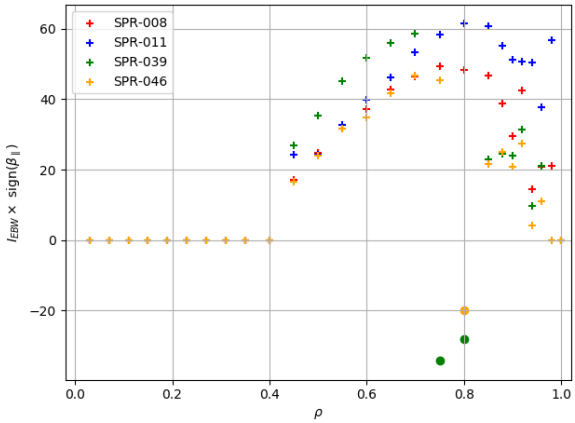

Figure 5. Total EBW driven current multiplied by the sign of the resonant electron velocity. Almost all runs show positive values implying the Okhawa effect is the dominant current drive mechanism.

Almost all SPRs show positive values meaning Okhawa is the dominant current drive mechanism. The only Fisch-Boozer dominant points occur in the region where SPR-039 and SPR-046 had numerical issues.

As STEP is a spherical tokamak there is a large trapped fraction due to the large variation in magnetic field strength between the low and high field side. This means the trapped-passing (TP) boundary occurs at small $\beta_\perp$ so the resonant interaction is likely to drive particles close to the TP boundary. We can investigate by looking at the deviation of the electron distribution function from Maxwellian after the absorption of the

EBW. The perturbation in the electron distribution function for SPR-008 at $\rho = 0.88$ for run giving the best current drive efficiency in Figure 6.

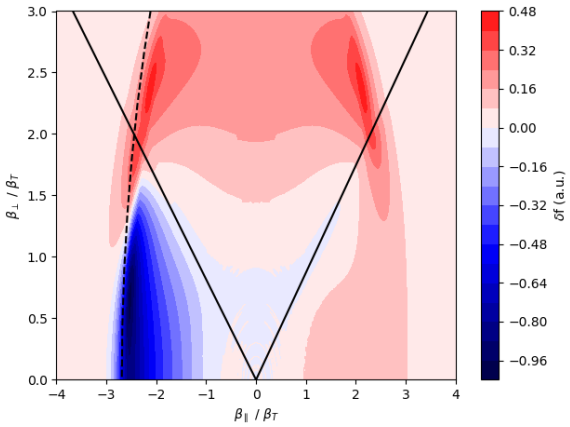

Figure 6. Perturbation in distribution function [a.u.] from Maxwellian at $\rho = 0.88$ for run giving the best current drive efficiency for SPR-008. $I_{CD} = -38.8$ kA, $N_\parallel = 0.64$ and absorption is on 2nd harmonic so Okhawa current drive is dominant. The resonance curve (dashed black) and trapped-passing boundary (solid black) are also shown.

The wave particle interaction has created an increase in density of electrons at higher $\beta_\perp$ near the downshifted resonance predicted in (3). Okhawa current dominates as the resonance is close to the TP boundary and large numbers of particles are trapped. Bounce averaging forces the distribution function to be symmetric in $\beta_\parallel$ inside the TP boundary, resulting in zero current. The fast bounce time of trapped electrons means momentum gets rapidly transferred across the TP boundary. This causes some de-trapping at the opposite sign of the resonant velocity which enhances the Okhawa effect [6].

5.3 Analysis of Absorption

The simple estimate of absorption (3) gives a prediction for the Y value where the EBW will be absorbed. This value is plotted against the value from GENRAY ray tracing in Figure 7. $\alpha = 3.35$ gave best fit.

There is reasonable agreement between the estimate and the predictions from GENRAY, with a mean absolute error of 0.02. This cannot replace GENRAY ray tracing calculations as it requires $N_\parallel$ and the magnetic field along the ray trajectory. We can use it to explain the switch from 1st to 2nd harmonic absorption and the change of sign in $N_\parallel$.

$N_\parallel$ increases over the ray trajectory, meaning $|N_\parallel|$ grows for rays starting with positive $N_\parallel$ and shrinks for rays starting with negative $N_\parallel$ as seen in Figure 8. The Doppler broadening of the harmonic therefore grows and shrinks during ray propagation for positive and negative starting $N_\parallel$ respectively.

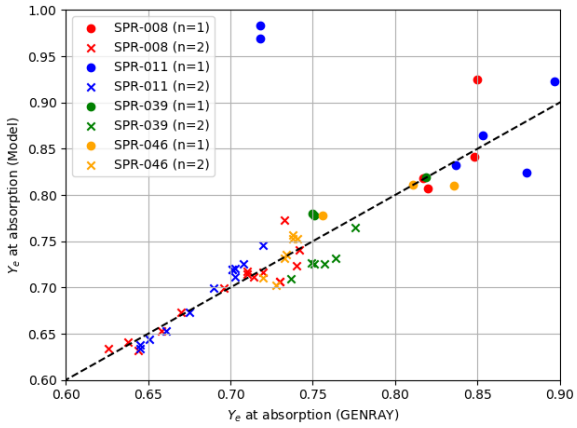

Figure 7. Predicted Y value at absorption using $\alpha = 3.35$ (y axis) vs value from GENRAY, for rays giving optimal current drive. The dashed black line is y=x. There is reasonable agreement with a mean absolute error of 0.02.

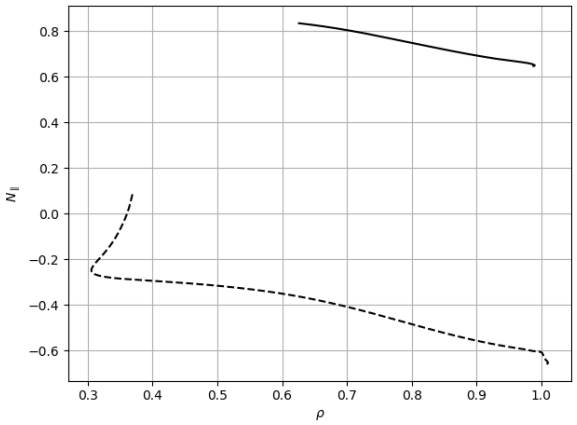

Figure 8. $N_\parallel$ evolution across the EBW ray trajectory for two rays giving maximum current drive at $\rho = 0.45$ (dashed) and $\rho = 0.75$ (solid) for SPR-008. Both rays start with $|N_\parallel| \sim 0.65$. The ray traces continue beyond the point of absorption but there is no power left in the ray.

When a ray meets the resonance condition it will be rapidly absorbed, so it is not surprising that rays with smaller $|N_\parallel|$ travel further into the plasma before being absorbed. Figure 9 shows the predicted absorption location vs launch frequency for SPR-008 and SPR-046 for $N_\parallel = 0.65$, a typical value after OXB conversion.

We see absorption on the 1st harmonic is only possible for $\rho < 0.9$ for a small range of frequencies unless $N_\parallel$ increases significantly. The magnetic well and the relativistic downshift of the resonance frequency reduces the possibility for 1st harmonic absorption and increases the possibility of 2nd harmonic absorption.

This explains the transition from 1st to 2nd harmonic absorption. We also see for SPR-008 the 1st harmonic is downshifted much further compared to SPR-046 due to the deeper magnetic well. This explains why 1st harmonic absorption was only possible for $\rho > 0.75$ at large $N_\parallel$ for SPR-046 but only seen for $\rho > 0.9$ in SPR-

008. In this region there is also no access to the 2nd harmonic at the launch frequencies examined.

The last observation to explain is that 2nd harmonic absorption gave higher current drive efficiency than 1st harmonic absorption in regions both were possible. This can be explained by the resonant interaction of the 2nd harmonic occurring at higher $\beta_\perp$ than the 1st harmonic, resulting in more efficient trapping as the resonant interaction is closer to the TP boundary.

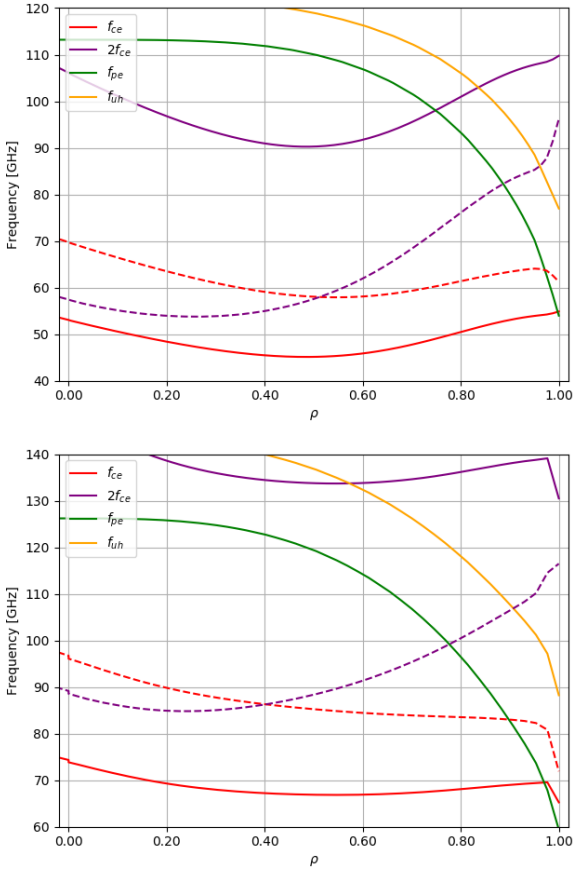

Figure 9. Estimate of EBW absorption on midplane for SPR-008 (top) and SPR-046 (bottom) for $N_\parallel = 0.65$. The cold 1st (red) and 2nd (purple) cyclotron harmonic frequencies and predicted 1st harmonic upshift / 2nd harmonic downshift from (3) (dashed) are shown. The plasma frequency (green) and upper hybrid frequency (orange) are also shown.

By estimating $N_\parallel$ and the ray trajectory we could also use (3) to identify frequencies and launch heights likely to give optimal access. It also can estimate the effect of changes in temperature on absorption which can be used to estimate EBW access for different plasma scenarios.

6 Summary

GENRAY and CQL3D were used to scan the EBW current drive efficiency for 4 STEP prototype reactor concepts. $\zeta_{CD} > 0.5$ was achieved for all scenarios for $\rho > 0.5$ and $\zeta_{CD} > 1$ is found for $0.6 < \rho < 0.9$. This is almost 3 times larger than the values found for EC. The EBW fails to penetrate the plasma beyond $\rho = 0.4$, though current drive becomes inefficient for $\rho < 0.5$.

The Okhawa effect is the most efficient mechanism for current drive in STEP. As STEP is a spherical tokamak the absorption of the EBW pushes electrons near or across the trapped-passing boundary preventing efficient Fisch-Boozer current drive.

EBW current drive occurs deepest in the plasma for rays starting with negative $N_\parallel$ and absorb on the 2nd harmonic. This is because $N_\parallel$ increases as the ray propagates inwards, reducing $|N_\parallel|$ for rays starting with negative $N_\parallel$ and reducing the size of the Doppler broadening of the cyclotron harmonics.

A simple estimate for the Doppler broadened EBW resonance is given. Due to the high temperature of STEP plasmas (Table 1), relativistic downshifts of the resonant frequencies due to mass increase are comparable with the Doppler shift. This means 1st harmonic absorption is only possible for $\rho > 0.75$ at large $N_\parallel$.

All current drive efficiencies should be considered optimistic as we have assumed 100% OXB coupling efficiency and neglected any effects due to finite beam width. In quoting current drive efficiencies, we have also assumed current drive is linear with power and ignored any non-linear effects of instabilities which occur at high power.

References

1. Smirnov, A. P., and R. W. Harvey. *CompX Report CompX-2000-01* (2001).
2. Harvey, R. W., and M. G. McCoy. *In Proceedings of the IAEA Technical Committee Meeting on Simulation and Modeling of Thermonuclear Plasmas*, pp. 489-526. 1992.
3. Decker, Joan, and Abhay K. Ram. *Physics of Plasmas* 13, no. 11 (2006): 112503.
4. Prater, Ronald. *Physics of Plasmas* 11, no. 5 (2004): 2349-2376.
5. Karney, Charles FF. *Computer Physics Reports* 4, no. 3-4 (1986): 183-244.
6. Decker, Joan. "Electron Bernstein wave current drive modeling in toroidal plasma confinement." PhD diss., Massachusetts Institute of Technology, 2005.
7. Preinhaelter, J., et al. In *AIP Conference Proceedings*, vol. 787, no. 1, pp. 349-352. American Institute of Physics, 2005.
8. Volpe, F., H. P. Laqua, and W7-AS Team. *Review of scientific instruments* 74, no. 3 (2003): 1409-1413.
9. Luce, T. C., et al. *Physical review letters* 83, no. 22 (1999): 4550.
10. Taylor, G., et al. *Physics of Plasmas* 11, no. 10 (2004): 4733-4739.
11. Saarelma, S., et al. *Physics of Plasmas* 26, no. 7 (2019): 072501.